Micromechanical based model for predicting aged rubber fracture properties

R. Kadri, M. Nait Abdelaziz, B. Fayolle, G. Ayoub, M. Ben Hassine, Y. Nziakou

Micromechanical based model for predicting aged rubber fracture properties

R. Kadri
Université de Lille, Unité de Mécanique de Lille – Joseph Boussinesq ULR 7512
M. Nait Abdelaziz (moussa.nait-abdelaziz@univ-lille.fr)
Université de Lille, Unité de Mécanique de Lille – Joseph Boussinesq ULR 7512
B. Fayolle
UMR CNRS 8006, Arts et Métiers ParisTech
G. Ayoub
University of Michigan Dearborn
M. Ben Hassine
Département MMC, EDF Lab
Y. Nziakou
Département MMC, EDF Lab

Research Article

Keywords: Aging, Rubber materials, Fracture properties, Micromechanical modeling, Damage

Posted Date: January 9th, 2023

DOI: https://doi.org/10.21203/rs.3.rs-2443096/v1

Additional Declarations: No competing interests reported.

Micromechanical based model for predicting aged rubber fracture properties

R. Kadri[1,2,3], M. Nait Abdelaziz[1*], B. Fayolle[3], G. Ayoub[4*], M. Ben Hassine[5], Y. Nziakou[5]

[1]*Université de Lille, Unité de Mécanique de Lille – Joseph Boussinesq ULR 7512, 59000 Lille, France*

[2]*Département MMC, EDF Lab, F-77818 Moret-sur-Loing, France*

[3]*Laboratoire des Procédés et Ingénierie en Mécanique et Matériaux (PIMM), UMR CNRS 8006, Arts et Métiers ParisTech F-75013 Paris, France*

[4]*Industrial and Manufacturing Systems Engineering, University of Michigan Dearborn, 48124 Dearborn, Michigan, USA*

[5]*Département MMC, EDF Lab, avenue des Renardières, F-77818 Moret-sur-Loing, France*

*** Corresponding authors:** moussa.nait-abdelaziz@univ-lille.fr

Abstract Environmental aging induces a slow and irreversible alteration of the rubber material's macromolecular network. This alteration is triggered by two mechanisms which act at the microscale: crosslinking and chain scission. While crosslinking induces an early hardening of the material, chain scission leads to the occurrence of dangling chains responsible of the damage at the macromolecular scale. Consequently, the mechanical behavior as well as the fracture properties are affected. In this work, the effect of aging on the mechanical behavior up to fracture of elastomeric materials, and the evolution of their fracture properties are first experimentally investigated. Further, a modeling attempt using an approach based upon a micro-mechanical but physical description of the aging mechanisms is proposed to predict the mechanical and fracture properties evolution of aged elastomeric materials. The proposed micro-mechanical model incorporates the concepts of residual stretch associated with the crosslinking mechanism and a so-called "healthy" elastic active chain (EAC) density associated with chain scission mechanism. The validity of the proposed approach is assessed using a wide set of experimental data either generated by the authors or available in the literature.

Keywords *Aging; Rubber materials; Fracture properties; Micromechanical modeling; Damage.*

1 Introduction

Rubber materials are used in a wide range of applications, prompted by their particularly high reversible deformations associated with low strength and their great damping and insulating properties. During operation, rubber materials are exposed to extreme mechanical and environmental perturbations, such as complex static and dynamic mechanical loadings, elevated temperatures, UV radiation, oxygen, and humidity. Therefore, understanding and modeling the operating conditions' influence on the mechanical and fracture properties is of high importance when designing structural rubber material components. Many experimental investigations showed the strong dependency of the mechanical and fracture properties of rubber materials on the loading condition history and on the chemical and physical aging exposure history. Those properties are directly influenced by the changes in the macromolecular network structure induced by a chemical processes that operate at the molecular scale (Dunn and Scanlan 1961; Colclough et al. 1968).

For the last few decades, many research investigations have focused on increasing our understanding of rubber materials' aging mechanisms and their effect on the mechanical properties. Different mechanistic and kinetic schemes of their thermo-oxidation process were proposed (Bolland 1949; Rincon-Rubio et al. 2001; Colin et al. 2019, 2021). A consensus among those studies describes the alteration of the macromolecular network structure by a three-step oxidation scheme: initiation, propagation, and termination. Initiation involves the creation of free radicals P°. The free radicals P° are extremely reactive with oxygen and consequently favor a chain reaction of chemical processes in the polymer, denoted as propagation. The termination consists in the transformation of the different radicals in the polymer

into inactive products like gas release or the creation of new crosslinks or chain scissions. These two competing mechanisms (crosslinking and chain scissions) modify the macromolecular structure of the polymer and play a significant role in the degradation of the mechanical properties (Fayolle et al. 2008; Planes et al. 2009; Belbachir et al. 2010; Le Gac et al. 2013; Howse et al. 2019; Bouaziz et al. 2020). The chemical composition, the macromolecular network structure, and the aging conditions of the rubber materials influence the relative predominance of the aforementioned aging mechanisms (Planes et al. 2010a).

With increasing aging time, a decrease of the fracture mechanical properties of rubber material whatever the degradation mechanisms is widely documented (Celina et al. 2005; Planes et al. 2009, 2010b; Le Gac et al. 2013; Pourmand et al. 2017; Kashi et al. 2018; Nait Abdelaziz et al. 2019).

Over the last century, a significant number of models were proposed to capture the macro-scale hyperelastic response of rubber materials. Based on their theoretical frameworks, we can differentiate between phenomenological and physical-based models. The phenomenological models provide a macroscopic description of the hyperelastic stress-strain behavior of rubber materials that is not connected to the macromolecular structure (Mooney 1940; Yeoh 1990). In physical-based models, we can distinguish between models describing the macromolecular network physics using Gaussian and non-Gaussian statistical approaches. The chains mechanics associated with the macromolecular network entropy decrease was described using a number of non-Gaussian-based theories . These non-Gaussian statistical theories account for the extensibility limit of randomly oriented molecular chains to capture the hyperelastic behavior of rubber materials using the probability distributions of (Jernigan and Flory 1969) and (Kuhn and Grun 1942).

It is worth mentioning that failure associated with the changes in conformational entropy was rarely accounted for through those approaches, and mainly the mechanical behavior and microstructural parameters evolution of rubber materials subjected to multiaxial loading conditions were considered (Vernerey et al. 2018; Bahrololoumi et al. 2020).

(Volokh 2007; Balakhovsky and Volokh 2012) proposed modifying the free energy potential, paving the way to coupling the macroscopic fracture with the constitutive modeling. The "energy limiter" approach theory is based upon an evident axiom: since a material cannot absorb an unlimited amount of energy, its value must be bounded by a maximum, thus a new free energy potential using the properties of upper gamma function was developed to consider rubber fracture property.

(Dal and Kaliske 2009) pointed out the incompetency of phenomenological and statistical hyperelastic models to account for rubber materials fracture. Accordingly, a modified entropic elasticity model describing the conformation capability of the chain and the energy of the interatomic bonds was proposed. The deformation and damage of a single chain coupled with advanced micro–macro transition (Miehe et al. 2004) enable the description of the finite-strain macro-response of rubber materials while using physical parameters.

Many other models describing the fracture of elastomeric materials can be found in the literature (Mao et al. 2017; Tehrani and Sarvestani 2017; Lavoie et al. 2019; Li and Bouklas 2020). They take different approaches which will not be discussed here. Indeed, the purpose of this work is modeling the impact of aging on fracture properties of rubber.

(Belbachir et al. 2010) studied the photodegradation effect on the mechanical properties of PLA and proposed a network alteration model by assuming that chain scission occurs mainly in the amorphous phase (rubbery phase). Later, (Rodriguez

et al. 2020) and (Ayoub et al. 2020) studied extensively the mechanism of photodegradation of semicrystalline polyethylene and developed a physically based composite-type model and introduced phenomenological damage evolutions of the macromolecular network to account for the alteration of the chemical and structural properties.

Macroscopic damage coupled with physical-based models introducing either a damage indicator or time-temperature equivalence approach were proposed to capture the effect of aging on the mechanical properties up to break (Belbachir et al. 2010; Nait Abdelaziz et al. 2019; Colin et al. 2019; Bahrololoumi et al. 2020; Kadri et al. 2022). In those models the experimentally measured molar mass between crosslinks M_c was established as a relevant indicator of damage induced by aging.

(Lake 2003) derived a useful relationship between the strain energy release rate (in the presence of a crack) and the molar mass M_c, which has been successfully applied when the crosslinking aging mechanism predominates. However, when chain scission is the prevailing aging mechanism, those models predict an increase in the failure energy with increasing aging-induced degradation, which is in contradiction with several experimental observations reported in the literature (Planes et al. 2009; Le Gac et al. 2013; Kashi et al. 2018). Indeed, chain scission mechanically increases the average value of M_c, leading to an increase of the strain energy release rate. Thus, the molar mass between crosslinks M_c cannot be adopted as a generalized damage indicator independently from the aging mechanism. This issue will be addressed in this work.

The purpose of this work is to develop a physically based micro-mechanical approach capable of predicting the effect of aging on the mechanical and fracture

behaviors of rubber materials regardless of the predominant degradation mechanisms. Physically based description of the aging mechanisms is proposed and coupled with the micromechanical model to accurately capture the experimental observations. The validity of the proposed approach is assessed using a wide set of experimental data either generated by the authors or available in the literature.

The paper is organized as follows: In section 2, the basic equations of the micro-mechanical model proposed by (Dal and Kaliske 2009) are reminded. Furthermore, in section 3, the micro-mechanical model is modified to account for aging. When crosslinking is predominant, a residual stretch concept is introduced to capture the degradation of the fracture properties. In the case of chain scission prevalent mechanism, a healthy and degraded subnetworks scheme is proposed to explain the aging effects on the fracture. In each case, experimental data allows to check the capability of the modified model to capture the evolution of the fracture properties. This capability is widely discussed whatever the aging mechanism. Finally, concluding remarks and perspectives are then drawn.

2 Theoretical background

The rubbery microstructure can be conceptualized hierarchically starting from the mesoscale with the macromolecular network enclosing a large number of randomly oriented, variable-length, and elastically crosslinked active chains and at the micro scale with the Kuhn segments. In this section the main features of the physically based micro-mechanical approach for describing the mechanical and fracture properties of elastomeric materials are given. It reposed on the mathematical framework proposed by (Dal and Kaliske 2009). Then, the model is extended to account for the degradation due to aging.

The highly nonlinear hyperelastic macroscopic behavior of rubber materials is associated with the decrease of the macromolecular network entropy. The behavior of the macromolecular network is achieved by combining the chain length statistics with a non-affine micro-macro transition using the micro-sphere model (Miehe et al. 2004). At the single-chain level, chains unfold with deformation, and they break when their limit of extensibility is reached. Therefore, the micromechanical behavior of a single polymer chain is achieved by accounting for the conformation capability of the chain and the energy of the interatomic bond (Dal and Kaliske 2009).

2.1 Micromechanics of a single polymer chain

The single polymer chain in the network is represented by a large number N of rigid segments (Kuhn segments) of length l, the total length of the unfolded chain being $L = N\,l$ (cf. Fig. 1).

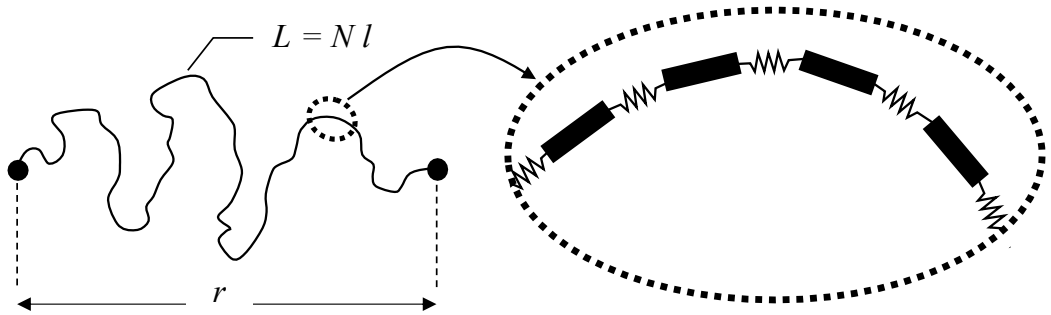

Fig. 1 Schematic representation of a single polymer chain with a magnified view representing interaction between Kuhn segments across bonds depicted by springs

In this framework, the links between the rigid Kuhn segments (represented by springs in Fig. 1) are capable of deforming, and therefore a mechanical energy is stored and released (energy of the interatomic bonds), which is in contrast with the classical mathematical descriptions. These links represent the covalent bonds between the repeating units of the chain (348kJ/mol for C-C) and result in the

polymer intrinsically exhibiting a high stiffness in the direction of the macromolecular chain.

Consequently, a simplified mechanical representation of the chain is therefore possible. The rheological model depicted in Fig. 2 represents each chain by a series of two springs: one capturing the energy storage resulting from the conformational change and the other the stored energy resulting from the interatomic displacement

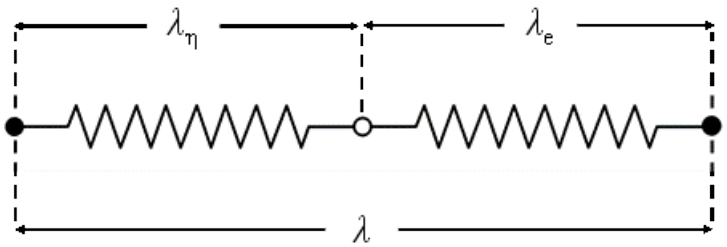

Fig. 2 Rheological representation of the model representing each chain

The hyperelasticity theory postulates the existence of a strain energy density ψ from which strains and stresses can be derived. This strain energy density corresponds to the Helmholtz free energy:

$$\psi = u - Ts = \psi_e + \psi_\eta \quad (1)$$

where u is the internal energy, T the absolute temperature, and s the entropy. An isothermal and isochoric deformation process induces a variation of the internal energy, resulting from the change in the interatomic distance, and of the entropy, resulting from the conformation evolution.

By correspondence with the rheological model described in Fig. 2, the internal energy corresponds to the energy stored by the interatomic bond and is noted ψ_e, while conformation capability of the chain in the network corresponding to the free energy density of the chain is noted ψ_η.

To describe the constitutive law associating the mechanical behavior of the chain conformations, we adopt in the modeling the well known form of the non-gaussian free energy density:

$$\psi_{\eta} = NkT\left(\lambda_r \mathcal{L}^{-1}(\lambda_r) + \ln\frac{\mathcal{L}^{-1}(\lambda_r)}{\sinh \mathcal{L}^{-1}(\lambda_r)}\right) \quad (2)$$

Where λ_r corresponds to the relative stretch of the chain $\lambda_r = \lambda_{\eta}.N^{(-1/2)}$, and $\mathcal{L}^{-1}(\lambda_r)$ is the inverse Langevin function, which can be evaluated through the Padé approximation:

$$\mathcal{L}^{-1}(\lambda_r) \approx \lambda_r \frac{(3-\lambda_r^2)}{(1-\lambda_r^2)} \quad (3)$$

The associated force (micro force of the entropic contribution) acting on a single chain by assuming Langevin statistics can be derived easily from eq.(2). It comes:

$$f_{\eta} = \frac{\mathrm{d}\psi_{\eta}(\lambda_{\eta})}{\mathrm{d}\lambda_{\eta}} = kT\lambda_{\eta}\left(\frac{3N-\lambda_{\eta}^{\,2}}{N-\lambda_{\eta}^{\,2}}\right) \quad (4)$$

Reminding that we are interested in modeling and predicting the fracture properties of aged elastomeric materials, the internal energy and the stretch associated with the interatomic bond cannot be neglected in the vicinity of the locking stretch i.e. the deformation limit. Accordingly, the constitutive equations describing the contribution of the interatomic bond to the total chain deformation is described using an expression derived from Morse potential (Dal and Kaliske 2009):

$$\psi_{\mathrm{e}} = e\left[\exp(-2\gamma) - 2\exp(-\gamma) + 1\right] \quad (5)$$

With:

$$\gamma = \alpha_1(\lambda_{\mathrm{e}} - 1) + \alpha_2(J-1)^2 \quad (6)$$

Where e corresponds to the dissociation energy for a pair of atoms, J = det **F** is the Jacobian, **F** being the deformation gradient and α_1 and α_2 are parameters controlling the slope of the energy drop.

The micro force associated with the internal energy contribution ψ_e acting on a single chain is expressed as follows:

$$f_e = \frac{\partial \psi_e}{\partial \lambda_e} = 2\alpha_1 e\left(-\exp\left(-2\gamma\right)+\exp\left(-\gamma\right)\right) \qquad (7)$$

Fig. 3 illustrates the evolution of the internal energy potential ψ_e and the associated micro-force f_e for a single chain.

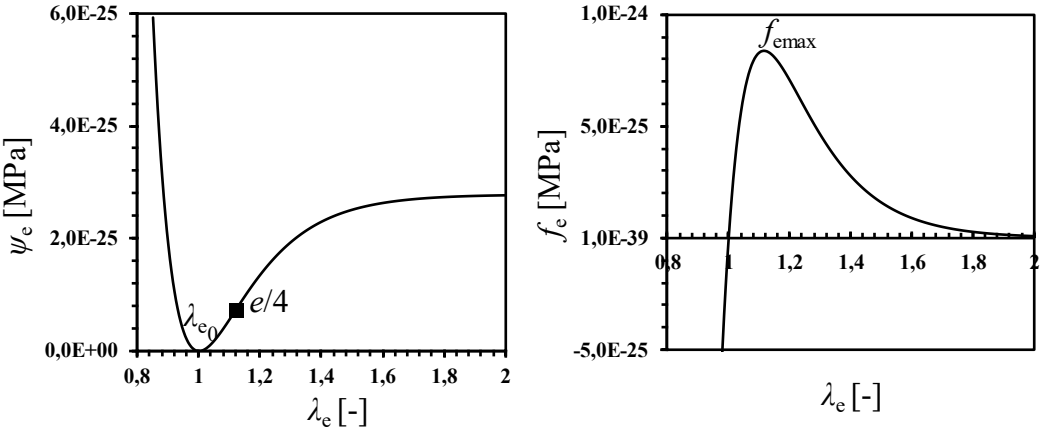

Fig. 3 Evolution of the internal energy ψ_e and corresponding micro-force f_e of a single chain. The parameter values used for generating these results are the following: e=3.34 10^{-24} MPa, α_1=9, α_2=5α_1

At the equilibrium (i.e. λ_e =1) ψ_e is null. On either side of this value, the energy increases up to infinity in the case of compression, and up to an asymptotic value for tension. Compression of the interatomic bonds associated with the folding of the chain, induces a negative micro-force f_e. When the chain is gradually stretched, the potential ψ_e decreases to reach a zero minimum value that is correlated with the equilibrium state λ_{e_0}= 1 and associated with a zero micro-force value. With further stretching of the chain (increasing λ_e), ψ_e and f_e increase. f_e reaches a maximum

value for $\lambda_{e_{max}}$, beyond which the chain breaks irreversibly. Due to the analytical form of ψ_e, at $\lambda_{e_{max}}$ the energy is equal to a quarter of the dissociation energy ($\psi_e(\lambda_{e_{max}}) = e/4$), which will be denoted as the threshold bond energy.

Above the glass transition temperature T_g, the mechanical response of rubbers is mainly associated with the change in entropy. This simplification is often assumed in classical hyperelastic modelling. However, the latter do not consider chains breaking, consequently the failure of the elastomer network.

Fig. 4 shows the evolution of the different energies during stretching: total energy ψ, internal energy ψ_e and the energy associated with the change of entropy ψ_η as function of the total stretch λ.

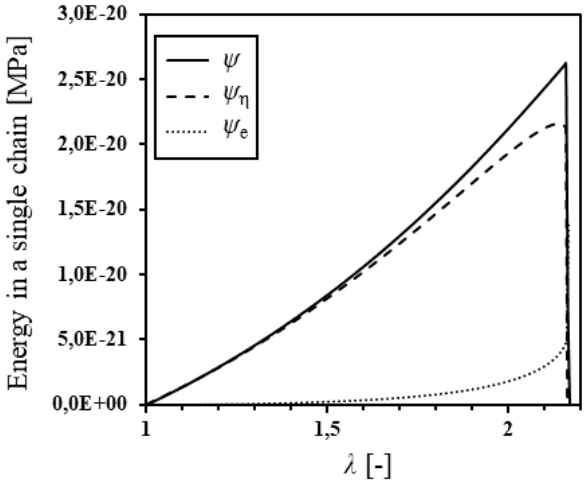

Fig. 4 Evolution of the total strain energy density ψ, of the entropic. contribution ψ_η, and of the bond energy ψ_e of a single chain as a function of the total stretch λ. The parameter values used for generating these results are the following: n=4.5 10^{20} cm^{-3}, N=10, $e/k.T$=3.44, α_1=9, α_2=5α_1

These evolutions are presented for qualitative comparison. It is clearly observed that the internal energy ψ_e is negligible compared with the entropic energy ψ_η, except when the global stretch is close to the locking stretch.

This can be explained by the deformation mechanism of the chain. Because of the weaker rotational stiffness of the Kuhn segments around the bond, the deformation process begins with the unfolding and orientation of the chain according to the stretch direction. This step mostly affects the entropic part of energy which is considered in the modeling across the Langevin spring. Once the chain is nearly unfolded, the extension of the interatomic bonds is initiated inducing the increase of internal energy ψ_e. Its deformation is captured by the second spring. This is allowed by the high stiffness of this spring compared to that of the Langevin spring. The total energy ψ is equal to the sum of the individual energies developed in each spring (ψ_η and ψ_e), while the stress acting on each spring is the same.

Thus, through this micromechanical modeling, the physics of a chain behavior up to and beyond the fracture can be well captured. paving the way to modeling the physical effects of aging on the rubbers fracture properties.

2.2 Macromolecular network model

The macromolecular network behavior is defined at the macro-scale and related to the mechanics and thermodynamics of continuum media by describing for each chain the deformation mechanisms through the above described rheological model (Fig. 2), and transitioning to the macro scale using the micro-sphere model (Miehe et al. 2004).

Rubber materials are generally assumed incompressible; therefore, the free energy function can be written in a volumetric-isochoric decoupled form:

$$\Phi = U(J) + \overline{\Phi}(\mathbf{g}; \overline{\mathbf{F}}) \quad (8)$$

Where $\mathbf{g}$ is the spatial metric, $\overline{\mathbf{F}} = J^{-\frac{1}{3}}\mathbf{F}$ corresponds to the isochoric part of the deformation gradient $\mathbf{F}$ that governs the isochoric stress.

Since for a single EAC, the free energy is given by eq.(1), the free energy of a macromolecular network $\overline{\Phi}$ is similarly decomposed and is expressed as follows:

$$\overline{\Phi} = n\,\psi_{\eta}\left(\lambda_{\eta}\right) + n\,\psi_{\mathrm{e}}\left(\gamma\right) \qquad (9)$$

Where n corresponds to the density of EAC per unit reference in the macromolecular network.

In the same way, the Kirchhoff stress is obtained by adding the hydrostatic and the deviatoric contributions:

$$\boldsymbol{\tau} = p\mathbf{g}^{-1} + \mathbf{P} : \overline{\boldsymbol{\tau}} \qquad (10)$$

Where $\mathbf{P}$ is the fourth-order identity tensor.

The hydrostatic stress p is obtained through the derivative of the volumetric part U of the free energy ($p = J\,\partial U\left(J\right)/\partial J$) where U is an incompressibility constraint that can take different forms (Horgan and Murphy 2009) and is considered as a penalty function to approach the incompressible response.

The deviatoric stress $\overline{\boldsymbol{\tau}}$ is derived from the isochoric part of the free energy function $\overline{\Phi}$ by using the intermediate derivative (i.e $2\partial\lambda/\partial\mathbf{g} = \lambda^{1-q}\,\mathbf{h}$ with $\mathbf{h} = \langle \overline{\lambda}^{q-2}\,\mathbf{t}\otimes\mathbf{t}\rangle$) (Miehe et al. 2004):

$$\overline{\boldsymbol{\tau}} = 2\frac{\partial\overline{\Phi}\left(\mathbf{g};\overline{\mathbf{F}}\right)}{\partial\mathbf{g}} = \overline{\Phi}'\,\lambda^{1-q}\,\mathbf{h} \qquad (11)$$

Where $\overline{\lambda}$ is the macro stretch and is related to the micro-stretch λ of a single chain through a q-root averaging over the unit micro-sphere ($\lambda = \langle\overline{\lambda}\rangle_{q}$), see (Miehe et al. 2004).

$\overline{\Phi}' = nf$ is the single elastic potential derivation and f is the micro force defined as $f = \partial\psi/\partial\lambda$.

Therefore, the isochoric contribution to macroscopic stress takes the following form:

$$\bar{\boldsymbol{\tau}} = n\left(f_{\eta} \frac{\partial \lambda_{\eta}}{\partial \lambda} + f_{e} \frac{\partial \lambda_{e}}{\partial \lambda} \right) \lambda^{1-q} \mathbf{h} = n\, f\, \lambda^{1-q} \mathbf{h} \qquad (12)$$

For more details about the mathematical developments of partial derivatives and calculation of stress see the appendix A.

Fig. 5.a illustrates the capability of the macromolecular network model to capture qualitatively the hyperelastic behavior of rubber materials beyond the fracture using the above equation. Furthermore, the evolution of the sub-stretches (λ_{η} and λ_{e}) during the mechanical loading are plotted in Fig. 5.b.

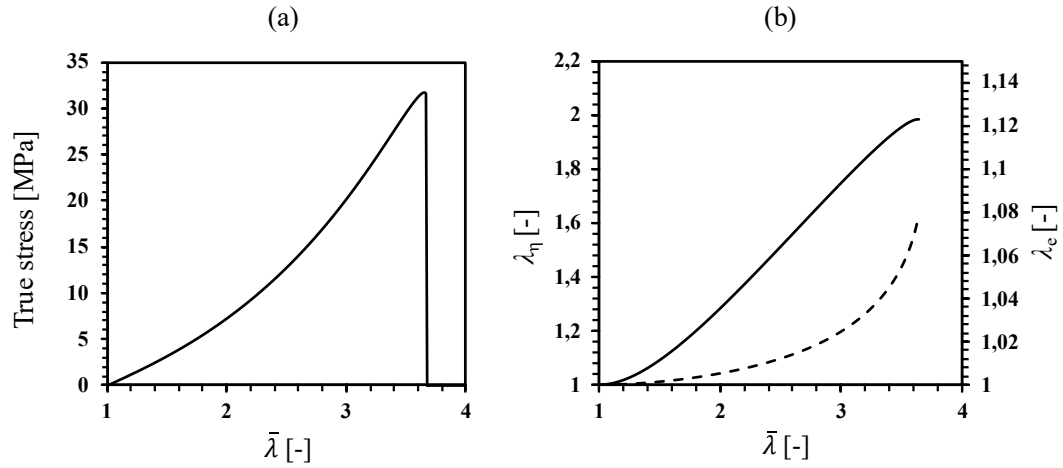

Fig. 5 (a) The true stress as a function of macroscopic stretch $\bar{\lambda}$, (b) evolution of the sub-stretches λ_{η} (solid line) and λ_{e} (dashed line) as a function of the macroscopic stretch $\bar{\lambda}$. The parameter values used for generating these results are the following: n=4.5 10^{20} cm^{-3}, N=10, $e/k.T$=3.44, α_1=9, α_2=5α_1

Fig. 5.b shows that the stretch associated to the bond energy λ_{e} is negligible at the beginning of the deformation and starts increasing when the molecular chains start aligning with the loading direction. It is important to note that λ_{e} exhibits lower values compared to λ_{η}, which is in correlation with the results presented in Fig. 4.

We can also conclude that the chain failure depends on the chain length and it occurs when the chain is fully stretched along the loading direction. At the molecular network level, the chain failure process depends on the statistical distribution of the chain length. This statistical distribution of chain length is accounted for through the non-Gaussian approach and the micro-macro transition carried out through the micro-sphere model.

Once these main features of the physically based model reminded, let us now pay attention to the consideration of the effects of aging.

3 Extension of the micromechanical model to account for aging

Environmental aging induces a slow and irreversible alteration of the rubber material's macromolecular network. This alteration is triggered by two mechanisms, crosslinking and chain scission, schematically illustrated in Fig. 6, which act simultaneously but one of them being generally predominant.

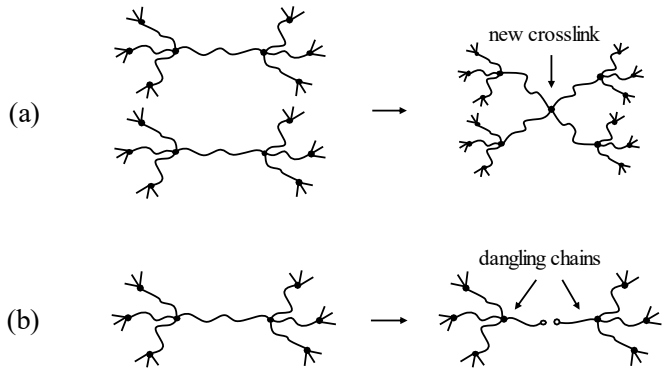

Fig. 6 Schematic representation of (a) crosslinking and (b) random chain scission

These two network alteration mechanisms influence the material behavior differently. Indeed, when crosslinking is the predominant mechanism, the EAC density n increases, which induces a decrease of both the average chain length N and consequently the maximum extensibility of the chains. Additionally, an early

hardening of the material is induced. This change in rigidity is generally well captured by assuming mass conservation (Marckmann et al. 2002; Ayoub et al. 2011a, b, 2020), which is expressed as follows:

$$n(t)N(t) = n_0 N_0 \qquad (13)$$

N_0 and n_0 being the values at the reference state (as received material) of the average chain length and the EAC density, respectively. The mass conservation principle was widely used in the literature to theoretically predict the mechanical behavior of rubber during aging. However, can the use of this principle alone be sufficient to predict both the mechanical behavior and rupture of the material? In this subsection, we suggest to address this issue by using our own experimental data.

Fig. 7 shows the evolution of the uniaxial tensile behavior of an EPDM material vulcanized by a peroxide compound at different aging periods at 150°C.

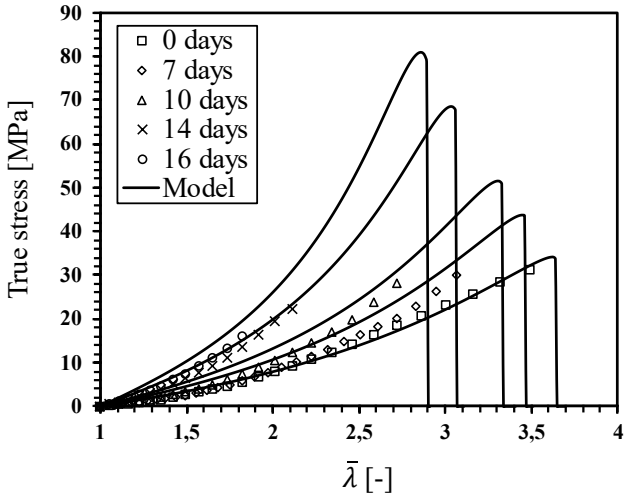

Fig. 7 Stress as a function of applied stretch for an EPDM aged at 150°C for different periods. The parameter values used for generating those results are the following: N=10, T= 296 K, e/kT= 3.44, q = 2, n_0=4.5 10^{20} (cm^{-3}), α_1=9, α_2=5α_1

The experimental data show an increase in the stiffness along with a decrease of the strain at break with increasing exposure time.

Furthermore, Fig. 7 presents a comparison between the proposed micro-mechanical model predictions assuming only mass conservation and the experimental data. The unaged test data material was fitted to identify the material parameters n_0 and N_0. Knowing the experimental evolution of the EAC density n (its determination will be explained further), the segment number N is deduced using the mass conservation given by eq.(13).

It is observed that the model only assuming mass conservation is able to capture the increasing stiffness with thermal aging. However, the model fails to predict the evolution of both stress and strain at break except for the reference state that is used to calibrate the parameters. Indeed, according to eq.(9), the free energy increases with the EAC density n. Because the material crosslinks, n increases, leading to an increase of both the stiffness and the network free energy. This mechanically induces an increase of the stress at break, which is in contradiction with the experimental observations, as depicted in Fig. 7. That demonstrates the inability to predict fracture by only using the mass conservation principle. A first issue to be addressed will be therefore to build a novel concept able to model the fracture process at the micro-scale.

When chain scission (cf. Fig. 6.b) is the predominant mechanism during aging, the EAC density n decreases. The mass conservation principle implicitly lead to an increase of Kuhn segments number N, and an decrease of the EAC density because $n(t).N(t)$ should remain constant. However, considering only mass conservation when chain scission is the predominant mechanism is a real issue because of the dangling chains which do not contribute neither to the stiffness nor to the fracture properties. How to estimate the real EAC density involved in the mechanical strength of the material? This is a second issue to be solved.

Moreover, the chain scission mechanism is accompanied by a decrease in EAC density n. Consequently, according to the mass conservation principle, the average chain length N increases, which theoretically provokes an increase of the strain at break (resulting from the dependency of λ_{lock} on N). This is in contradiction with the experimental observations reported by many available investigations (Planes et al. 2009, 2010b; Le Gac et al. 2013; Kashi et al. 2018). Hence, mass conservation cannot be used to predict either the mechanical behavior or the fracture for this aging mechanism.

To partially conclude, the assumption of only mass conservation is not suitable to describe:

a. The fracture properties of rubbers when crosslinking is the aging mechanism
b. both the evolution of the mechanical behavior and the fracture properties when chain scission is the aging mechanism

Since the mechanisms of crosslinking and chain scission are physically different, a unified theory that aims to capture the physical effects of both aging mechanisms on the behavior of rubber materials up to failure is difficult to conceive. Therefore, in this work we develop and propose approaches respectively suited to each mechanism, which allows to capture the aging effects on the behavior of rubber materials up to failure. Keeping in mind that few works deal with the problem in literature, and more particularly with the effect of chain scission mechanism on the evolution of failure properties, a novel theoretical framework for the modelling of ageing mechanisms and their impact on the mechanical and fracture properties is proposed and detailed in what follows.

3.1 Crosslinking mechanism

3.1.1 Residual stretch concept

Crosslinking mechanism lead to increase EAC density n in the network and simultaneously to the reduction of chain lengths N via the creation of new crosslinks. Understanding of what happens at the microscale being unavoidable to explain the macroscopic observations, we have attempted the described below reasoning which led us to propose a residual stretch theory.

When crosslinking operates, it creates new crosslinking nodes in the rubber network increasing over time the density of rubber network, as schematized in Fig. 8.a. The increase of the density network leads at the same time to a shortening of EAC length, schematically described in Fig. 8.b. To ensure the mechanical balance of the network during the shortening of chains induced by crosslinking, residual micro-stresses are involved at the chain scale, represented by arrows in Fig. 8.b. Higher the shortening of the chain, higher the residual stress. These residual stresses operate at the chain scale and lead to the stretching of the interatomic bonds. This residual micro-stretching reduces the energy capability of the bonds to absorb mechanical loadings and causes the alteration of fracture properties of rubber network during aging.

We can conclude that the increase of the crosslinking density induces residual stretches at the microscale. The network entropy decrease is accompanied by a progressive stretching of the network chains, as schematically represented in Fig. 8. Therefore, the remaining conformation capability of the chain in the network is reduced.

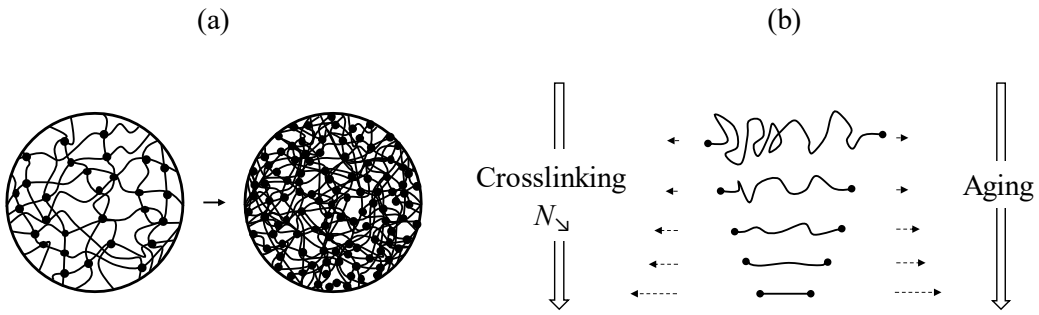

Fig. 8 Schematic representation of (a) the network densification and (b) chain stretching at the microscale induced by an increase of the crosslinking density

To formalize this argument, we consequently developed the concept of residual stretch which is represented schematically in Fig. 9. Considering the unaged material as the initial state (Fig. 9.a), we postulate the existence of an intermediate state that represents the effect of aging on the chain (central frame in Fig. 9.b). Let us remind that this intermediate state is the consequence of the residual stretching of interatomic bonds constituting the chain, which originates from the increasing crosslinking density of the network and implicitly the chains shortening during aging. Therefore, this residual stretch is incorporated into the micromechanical model by adding to the initial state a micro-stretch λ_{res} (which depends on the amount of aging), before applying the external load. Finally, for material can be loaded again, the intermediate state is updated creating a new reference state representing the aged material which is degraded compared with the as received one.

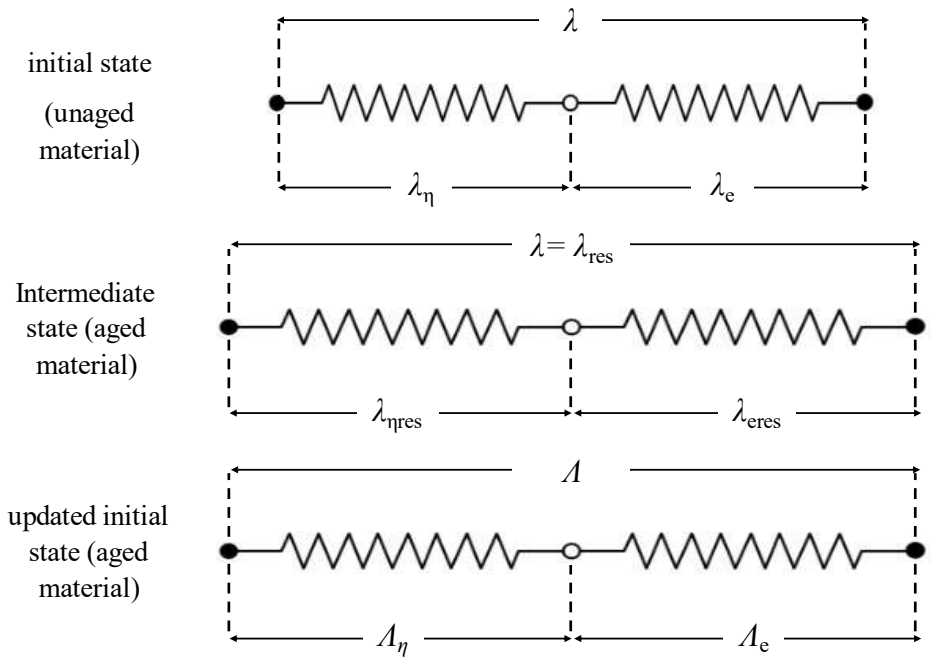

Fig. 9 Schematic representation of the modified model to account for crosslinking and the induced residual stretch

The aging-dependent residual micro-stretch is assumed dependent on the actual EAC or more precisely on the normalized ratio n/n_0 and is written in the following general form:

$$\lambda_{res} = \left(\frac{n}{n_0} \right)^c \tag{14}$$

With n and n_0 being the current and the initial EAC density, respectively. The parameter c is a macro-micro non-affinity parameter, which allows linking the degradation of the network at the macro scale to the micro-stretching at the chain scale ($\lambda_{\eta_{res}}$ et $\lambda_{e_{res}}$). For the as-received rubber material, $\lambda_{res} = 1$; hence, no residual micro-stretch is applied.

Accordingly, a numerical implementation scheme of the model has been built and is detailed in Table 1.

Table. 1 implementation scheme of the model

1.	Deformation gradient **F** (uniaxial tension mode), discrete orientation vectors $\mathbf{r}^i$ with their respective weight w^i for the micro sphere integration point *m*. see (Miehe et al. 2004)
2.	Compute the non-affine stretch see (Miehe et al. 2004)
	$\mathbf{t}^i = \bar{\mathbf{F}}\,\mathbf{r}^i$ (Eulerian orientation vector of a given single chain)
	$\bar{\lambda}^i = \left\|\mathbf{t}^i\right\|$ (stretch of a given single chain)
	$\lambda = \left[\sum_{i=1}^{m}\left(\bar{\lambda}^i\right)^q w^i\right]^{1/q}$ (average network stretch)
3.	Update the stretch to prestretch the system: aging crosslinking mechanism effects
	$\lambda = \lambda_{\text{res}}$
4.	Internal equilibrium iteration
4.a	Properties of rheological representation
	$\lambda_\eta^0 = \lambda_{\text{res}}$ and $\lambda_e = \frac{\lambda_{\text{res}}}{\lambda_\eta}$
	λ_η is the unknown of the problem
4.b	Residual equation
	$r = f_\eta\,\lambda_\eta - f_e\,\lambda_e \approx 0$
	Equation to solve with any numerical method (we use Newton-Raphson method)
4.c	Newton-type iteration
	$\lambda_\eta^{k+1} = \lambda_\eta^k - \frac{r}{r'}$

Where $r' = \dfrac{\partial r}{\partial \lambda_\eta}$

Allow to identify values of λ_η and λ_e for each load increment

5. Update the reference state

$$\Lambda = \Lambda_\eta = \Lambda_e = 1$$

With

$$\Lambda = \frac{\lambda_{res}^k}{\lambda_{res}^1}, \quad \Lambda_\eta = \frac{\lambda_\eta^k}{\lambda_\eta^1} \quad \text{and} \quad \Lambda_e = \frac{\lambda_e^k}{\lambda_e^1}$$

6. Compute the micro-forces

$$f_\eta = kT\Lambda_\eta \left(\frac{3N - \Lambda_\eta^2}{N - \Lambda_\eta^2} \right)$$

$$f_e = 2\alpha_1 e\left(-\exp\left(-2\gamma\right) + \exp\left(-\gamma\right)\right)$$

$$f = \frac{f_\eta \bar{\square}_e + f_e \bar{\square}_\eta}{\Lambda_\eta \bar{\square}_\eta + \Lambda_e \bar{\square}_e} \text{ (see appendix A)}$$

7. Compute macro-stress

$$\boldsymbol{\tau} = \boldsymbol{\tau}_{iso} + \boldsymbol{\tau}_{vol}$$

Where $\boldsymbol{\tau}_{iso} = \mathbf{P} : \bar{\boldsymbol{\tau}}$ and $\boldsymbol{\tau}_{vol} = p\mathbf{g}^{-1}$ refer to eq.(10)

The effect of the residual stretch on the fracture behavior of the rubber can be explained through the effect of crosslinking on the macromolecular network. Indeed, the reduction of chains length induces a decrease in the network entropy and elongation at break. The relevance of the concept of residual stretch is demonstrated in Fig. 10 which represents the evolutions during aging of entropy and bond residual micro-stretching $\lambda_{e_{res}}$ of an EPDM chain at 150°C (Fig. 10.a), as

well as the influence of bond residual micro-stretch $\lambda_{e_{res}}$ on the macroscopic failure strain (Fig. 10.b).

Fig. 10.a shows that the more the aging of the EPDM network progresses, the more the chain entropy decreases because of the decrease of the chain length. In the same time, chain shortening induces an increase of the bond residual micro-stretching $\lambda_{e_{res}}$. The consequence at the macroscale is shown in Fig. 10.b, the increase in $\lambda_{e_{res}}$ involves a decrease of the macroscopic fracture strain which agrees with experimental observations. Therefore, the proposed micro-scale approach allows capturing the complex macromolecular network degradation resulting from chains crosslinking and its effects on the fracture properties.

Precising that in the modeling, the value of energy dissociation of a pair of atoms (cf. eq.(5)) is always the same during aging. Indeed, aging does not affect its value.

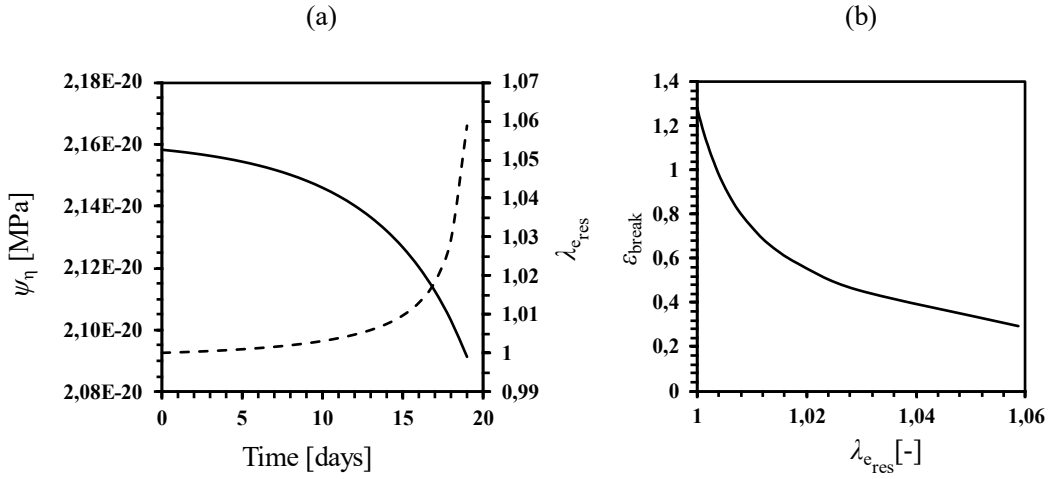

Fig. 10 Evolution of entropy and of bond micro-stretching of an EPDM chain during thermo-oxidative aging at 150 °C (a), influence of bond micro-stretching on the evolution of true strain at break (b)

Fig. 11 presents a comparison between the micromechanical model predictions and the experimental uniaxial tensile behavior of EPDM material vulcanized by using a peroxide compound and aged at 150°C for different time exposures (Kadri et al.

2022). These results must be compared to that presented in Fig. 7 while assuming only the mass conservation principle. It is observed that the modified micromechanical model is able to capture the mechanical response and its alteration with thermal aging. In contrast with results presented in Fig. 7, the micromechanical model is successful in capturing the evolution of both stress and strain at break, which is clearly an improving and a highlights contribution of this work.

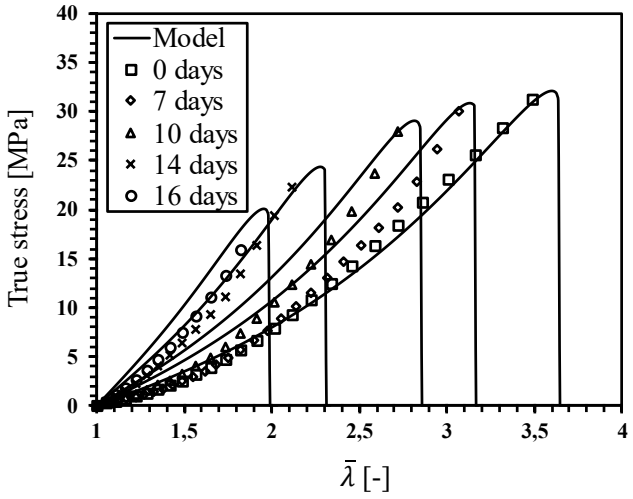

Fig. 11 Comparison between the experimental stress vs. stretch and the modified micromechanical model predictions for an EPDM aged at 150°C at different aging periods

3.1.2 Experimental data and computational results

a) Experimental data

In this work, both experimental data generated by the authors and extracted from the literature are used to discuss the validity of the proposed approach and to justify the suggested model modifications. For that purpose, two ethylene propylene diene monomer EPDM rubber were involved in the experimental investigation. The first one (denoted EPDM 01) is vulcanized by using a peroxide compound, and is widely used for thermal insulation, The second one (denoted EPDM02) is vulcanized using a sulfur compound (Nait Abdelaziz et al. 2019) and is used to manufacture electrical junctions. Sulfur vulcanization allows obtaining a high deformability of the rubber.

The experimental data were generated by the authors and the EAC density evolution of the EPDM network was identified by using swelling tests[1] (Nait Abdelaziz et al. 2019; Kadri et al. 2022) .

Thermo-oxidative aging was achieved by exposing the EPDM materials (noted EPDM01 and EPDM02) samples to variable aging periods at the following temperatures: 90, 110, 130 and 150°C in air-ventilated ovens for EPDM01 and 130, 150, 170°C for EPDM02. The tensile tests on EPDMs samples were carried out using an Instron device equipped with a 1kN load cell under a crosshead speed of 50mm/min and at ambient temperature. The tests were conducted according to ISO 37:2011 using H3 specimen geometry of 2mm thickness. To evaluate the material scattering, seven samples were tested for each aging condition.

b) Alteration kinetics

Based on the previous discussion, EAC density $n(t)$ is considered as the best indicator for describing the degradation of the macroscopic network. The evolution of the EAC density $n(t)$ is approximated by using an exponential law[2] (using least squares method) which parameters are summarized in appendix B.

Fig. 12 presents the evolution of the EAC density n of the studied materials at the reference temperature (150 and 170°C for EPDM01 and EPDM02 respectively). The EAC density n monotonically increases with time, which is the marker of a predominant crosslinking mechanism during thermo-oxidative aging.

---

[1] For EPDM rubber $n(t)$ was determined experimentally using swelling tests, which consist of immersing a rubber sample in a suitable solvent. This kind of reversible experiment allows estimating the elastically active chains (EAC) concentration (Kraus 1963).

[2] The evolution of the EAC density n(t) is approximated by using the following general exponential form: $n(t) = b_1 . \exp(b_2.t) + b_3 . \exp(b_4.t)$, where b_i are fitting parameters.

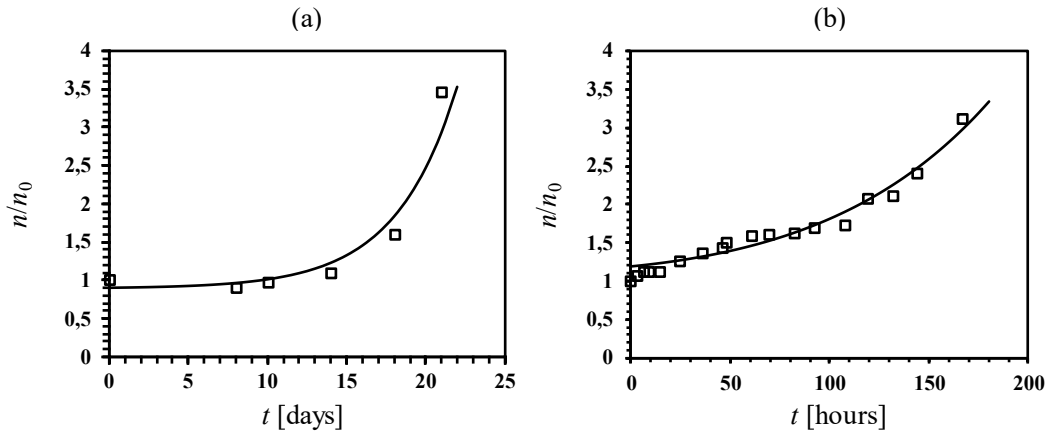

Fig. 12 Evolution of the EAC density n (mean values) during aging at reference temperature as a function of aging time (in days) for (a) EPDM01 and (b) EPDM02 materials (Nait Abdelaziz et al. 2019; Kadri et al. 2022)

c) Fracture properties prediction

The predictive capabilities of the model to capture the evolution of fracture properties are discussed in this section. Since the aging of EPDM rubbers is here predominantly controlled by crosslinking mechanism, only the parameter c of eq.(14) needs to be additionnaly identified. This identification is conducted by using the experimental fracture strains at the reference temperature (150°C). The whole model parameters are summarized in table 2.

Table. 2 parameters values of the constitutive model

Model parameter	EPDM01	EPDM02
n_0 [cm^{-3}]	4.5 10^{20}	1.09 10^{20}
N	10	16
e [MPa]	1.8 10^{-20}	1.8 10^{-20}
α_1	9	6
q	2	3.5
c	0.8	0.6

The predictive capability of the model is now assessed by comparing the model predictions and the experimental fracture properties of the studied materials aged at

different temperatures and periods. For that purpose, we used the time-temperature equivalence approach (the Arrhenius power law[3]) to unify the material data of different aging temperatures (Nait Abdelaziz et al. 2019), allowing to build the master curves of stress and strain at break. The parameter that needs to be identified for the Arrhenius power law parameter is the activation energy, which was found equal to E_a = 95 and 110kJ/mol for EPDM01 and EPDM02 respectively.

The evolution of the ultimate properties (strain and stress at break) of EPDM01 material as a function of reduced aging time at different aging temperatures is plotted in Fig. 13. The experimental data for different aging temperatures and periods are presented as dots, while the model is presented as a solid line.

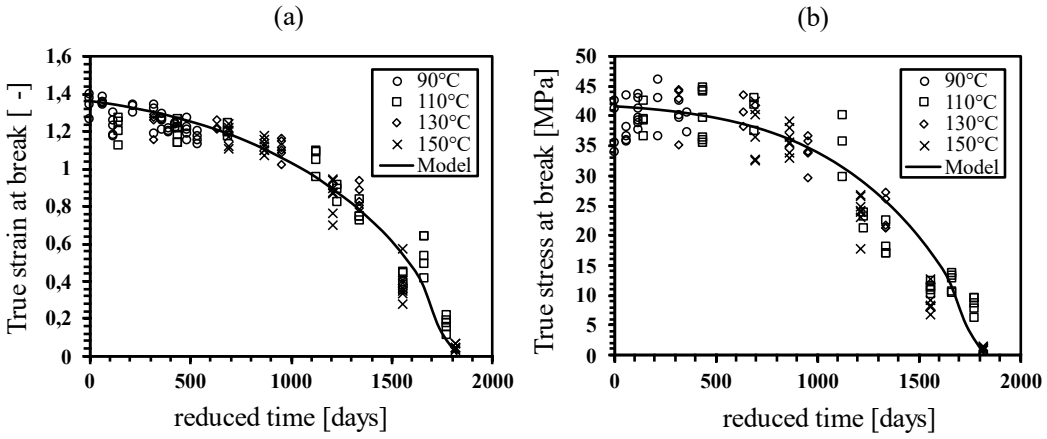

Fig. 13 (a) True strain and (b) true stress at break as a function of the reduced time for EPDM01 material

It is clearly shown that the modified micro-mechanical model introducing the concepts of residual stretch due to crosslinking mechanisms allows capturing the experimental data evolution. Indeed, we notice a good agreement between the

[3] The Arrhenius-based shift factor a_T takes the following form: $\ln(a_T) = -\frac{E_a}{R}\left(\frac{1}{T} - \frac{1}{T_0}\right)$, where E_a is the activation energy, T is the absolute temperature, T_0 is the reference temperature, and R is the perfect gas constant.

experimental fracture properties, in terms of either stresses or strains at break, and the model. The experimental data form a scatter around the model, proving the validity of our proposed approach. This ability is confirmed when analyzing the results for EPDM02 (Fig. 14)

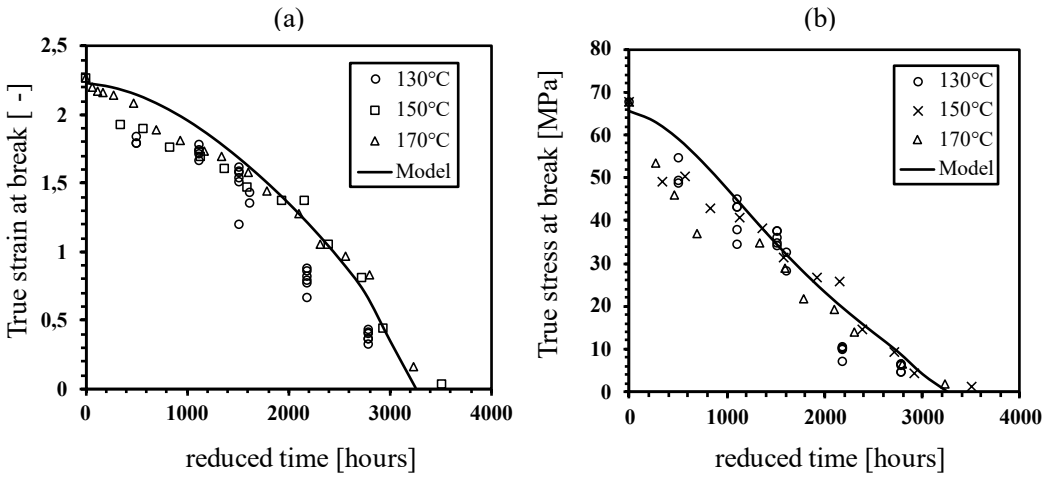

Fig. 14 (a) True strain and (b) true stress at break as a function of the reduced time for EPDM02 material

3.2 Chain scission mechanism

(Mark and Tang 1984) studied the effect of bimodal networks (i.e networks which are composed of chains statistically exhibiting two length average values) on the mechanical properties of rubber materials. It was reported that when long chains are predominant compared to small chains, the fracture is primarily controlled by the first ones. Paradoxically, (Planes et al. 2009) reported a decrease in strain at break in the case of chain scission which is contradictory, because the increase of the chain length theoretically induced by this mechanism should involve an increase of the strain at break which is proportional to $N^{1/2}$. It was also reported in this work that a multimodal distribution of the chain length cannot explain these conflicting observations. The decrease of the strain at break experimentally observed was

however explained by the presence of sub-networks with different chain lengths. Two architecture network properties were identified to control the overall mechanical behavior: load bearing subnetwork and weakened zones comprising large free agglomerates which do not contribute to the stiffness.

3.2.1 Healthy and degraded subnetworks scheme

The creation of dangling chains resulting from chain scission mechanism induces a decrease of EAC density n. Consequently, according to these experimental observations, we assume that the subnetworks created during aging can be classified in two types: the first which contribute to the stiffness (load bearing network) and denoted "healthy" subnetwork, the second which can be considered as a "degraded" subnetwork which do not take part to the mechanical strength. In fact, even if the "degraded" subnetworks contains EAC, these latter cannot fully contribute neither to the mechanical stiffness nor to the fracture process because they are surrounded by dangling chains (cf. Fig. 15). Indeed, this heterogeneity in terms of subnetworks modifies the stress distribution, the load being essentially transmitted through the "healthy" zone. When breakage occurs, only the "healthy" part of the network is involved. Thus, because of these dangling chains, the mass conservation principle must be suited to account for the two kinds of subnetworks and can be rewritten as $n_0 N_0 = n_{he} N_{he} + n_{de} N_{de}$.

Where the subscript "he" and "de" corresponds to the "healthy" and "degraded" subnetworks respectively.

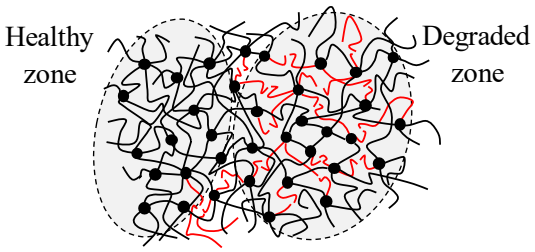

Fig. 15 Schematic representation of the bimodal network induced by chain scission during aging (dangling chains in red)

In what follows we assume that only the healthy EAC density n_{he} is involved in the fracture process. Moreover, during aging, the average chain length N_{he} is not affected and keep the initial value N_0. Indeed, there is no reason for the average chain length to evolve during aging, since the chain scission mechanism tends to make them inactive.

Assuming the above considerations, a "healthy" EAC density n_{he} is therefore introduced as a damage indicator to capture the evolution of the fracture properties when chain scission is the predominant mechanism. This healthy EAC density n_{he} is expressed in the following simplest form:

$$n_{he} = n_0 \frac{n - n_{th}}{n_0 - n_{th}} \qquad (15)$$

n_0 corresponds to the unaged material EAC density, n_{th} corresponds to the threshold EAC density below which the material is supposed to be completely degraded (meaning that no load can be borne), and n is the overall EAC density determined experimentally.

3.2.2 Experimental data and computational results

a) Experimental data

To discuss the validity of the proposed approach and to justify the suggested model, experimental data extracted from the literature are used. For that purpose, two rubber materials are analyzed: (a) A polyether-based polyurethane PU: the experimental data were generated by (Le Gac et al. 2013), and (b) a silicone rubber SR: the experimental data were generated by (Kashi et al. 2018). Swelling tests results were not available for those materials. Therefore, the EAC density was deduced from tensile tests through the shear modulus value.

PU specimens were aged during 18 months at 70, 90, 100, 110, and 120°C in sea water renewed every day. The accelerated thermo-oxidative aging of SR was achieved by immersing the specimens in beakers filled with polyalkylene glycol (PAG) oil and placed in an oven at 195°C over 6 weeks. Aged PU material tests were performed using ISO 37-standard samples of 2mm thickness. The tests were conducted under a crosshead speed of 50mm/min. Before mechanical testing, samples were stored for 24h in sea water at room temperature (Le Gac et al. 2013). The mechanical measurements on aged SR samples were achieved at ambient temperature using a crosshead speed of 200mm/min. The strain measurements were achieved by using a contactless extensometer. For each batch, three dumbbell-shaped specimens were tested.

b) Alteration kinetics

Like for EPDM material, the evolution of EAC density $n(t)$ was approximated by using an exponential law (least squares method). Those parameters for each studied material are summarized in appendix B.

The EAC density n was identified via the measure of the shear modulus μ by using the experimental tensile tests, n being deduced through the following relationship: $\mu=nkT$. Where k is the Boltzmann constant, T the absolute temperature.

Fig. 16 presents the evolution of the EAC density n of the studied materials. Only the EAC density n of the reference temperatures (120°C) are presented for PU material. The numerical evolution of the EAC density is presented by a solid line. Fig. 16 shows a decrease of EAC density regardless of the material, revealing a predominant chain scission degradation mechanism during aging.

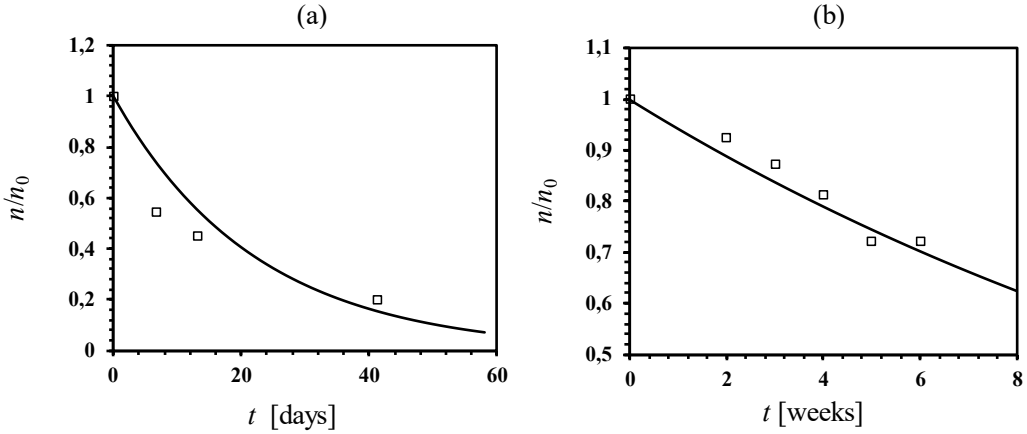

Fig. 16. Evolution of the EAC density n during aging as a function of aging time (in days or weeks) for (a) PU (120°C) and (b) SR (195°C) materials

c) Fracture properties prediction

Since the environmental aging of SR and PU rubbers is predominantly controlled by chain scission mechanism only the parameter n_{th} is to be additionnaly identified. The parameters n_{th} were identified on the experimental fracture strains at the reference temperatures. The remaining model parameters were identified by fitting the true stress-true strain curves of the unaged materials and are summarized in table Table. 3.

Table. 3 Values of different parameters of the constitutive models.

Model parameter	PU	SR
n_0 [cm^{-3}]	1.9 10^{21}	5.12 10^{19}
N	120	345
e [MPa]	1.25 10^{-20}	7.15 10^{-19}
α_1	7	7

q	2	2
n_{th} [cm^{-3}]	3.8 10^{20}	3.5 10^{19}

For SR material, only one set of data at 195°C is available, hence, the model results are only calibration. The purpose of using SR data in the validation is to show the capability of the proposed approach to capture the evolution of the mechanical behavior of different rubber materials.

To assess the predictive capability of the model, a comparison with the experimental fracture properties of the studied materials aged at different temperatures and periods is achieved. For that purpose and like previously for EPDM material (section 3.1), we have built a master curve using the time-temperature equivalence approach (the Arrhenius power law) that unifies the data of PU material for different aging temperatures. The activation energy for this material was found equal to E_a = 120 kJ/mol. Since only one aging temperature is available for the SR material, the time-temperature equivalence principle cannot be used.

The evolution of the ultimate properties in terms of stress at break as a function of aging time at different aging temperatures is plotted in Fig. 17. It is clearly shown that the modified micro-mechanical model introducing the concepts of the "healthy" EAC density allows capturing the experimental evolution.

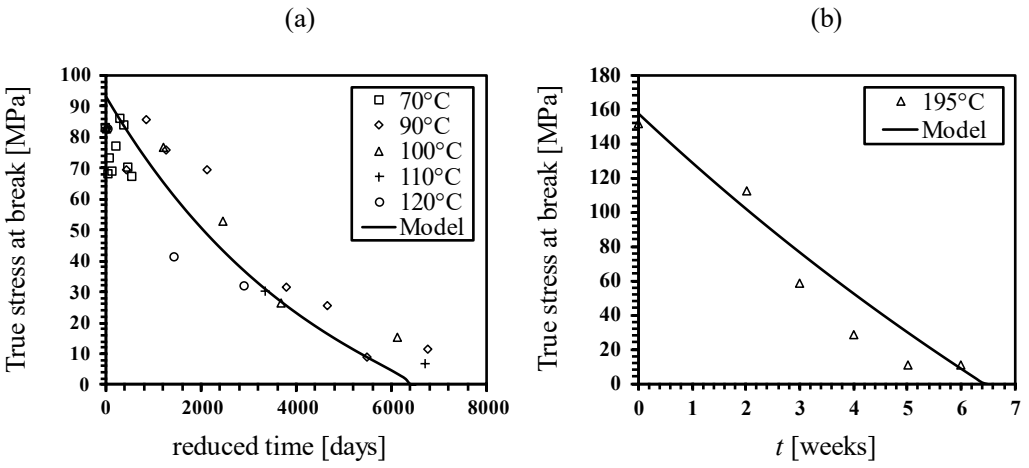

Fig. 17 True stress at break as a function of (a) the reduced time for PU and (b) the time (in weeks) for SR

Fig. 17.a and Fig. 17.b present the true stress at break as a function of the reduced aging time for PU and aging time for SR material. The dots represent the experimental data while the solid line is for the model.

The experimental data are arranged around the model. It is clearly shown that the modified micro-mechanical model leads to satisfactory estimates when compared to the experimental data, especially given the simple linear form of eq.(15). That can be surely improved but it requires more experimental data on materials exhibiting chain scission during aging.

Moreover, either for crosslinking observed for EPDM material or chain scission in the case of PU material, the predictive capability was demonstrated since the parameters were identified at a reference temperature, the results for the other temperatures being model predictions.

4. Discussion

In this work, the behavior of aged rubber materials up to fracture is modeled using a coupling between the physically based description of the aging mechanisms and the micro-mechanical model based on the (Dal and Kaliske 2009) approach.

Specifically, the macromolecular network behavior is defined at the macro-scale and related to the mechanics and thermodynamics of continuum media by describing for each chain the deformation mechanisms and the effect of thermo-oxidative aging and transitioning to the macro scale using the micro-sphere model (Miehe et al. 2004). The rheological representation of the model describes each chain by a series of two springs capturing the energy storage resulting from the deformation-induced conformational change and the stored energy resulting from the interatomic displacement. Environmental aging induces a slow and irreversible alteration of the rubber material macromolecular network. This alteration is triggered by two mechanisms, crosslinking and chain scission, which act simultaneously but with one generally being predominant (Belbachir et al. 2010); (Nait Abdelaziz et al. 2019). When crosslinking is the predominant mechanism, the EAC density increases, which induces a decrease both of the average chain length N and consequently of the maximum extensibility of the chains. Furthermore, it involves at micro-scale a pre-stretching of the chains, this residual stretch being aging dependent. This residual stretch is incorporated into the macromolecular model by adding a micro-stretch to the initial state before applying the external load. When chain scission is the predominant mechanism during aging, the EAC density decreases. In this work, we assume that the network becomes heterogeneous with the presence of sub-networks with different chain length denoted as “healthy” and “degraded” zones. Indeed, this heterogeneity at the microscale modifies the stress distribution, the load being transmitted essentially through the “healthy” zone. Taking into account the above considerations, the noted “healthy” EAC density is therefore introduced as a damage parameter to capture the evolution of the fracture properties when chain scission is the predominant mechanism. The validity of the proposed approach is assessed using a wide set of experimental data

generated by the authors and available in the literature. The comparison between the experimental and the computational results demonstrates the predictive capability of the model to capture the evolution of the mechanical and fracture properties of aged rubbers whatever the aging mechanism.

Rubber materials are highly viscous materials, and understanding the effect of aging on the viscosity is of high interest. The viscosity in rubbers is associated with the chain reptation mechanisms, which are associated with the thermal motion of chains and entanglements. Hence the chain length influences the rate of chain reptation, and therefore the degradation of the macromolecular network in theory affects the viscosity. The effect of aging on the viscosity needs to be considered by first understanding this effect through an extensive experimental investigation and second by including viscosity in the proposed model.

As a perspective, in the same way that proposed by (Trapper and Volokh 2010) such a modeling can be implemented in a FE software to simulate the process of crack propagation due to aging. An attempt of its feasibility has been achieved showing promising results (Fig. 18)

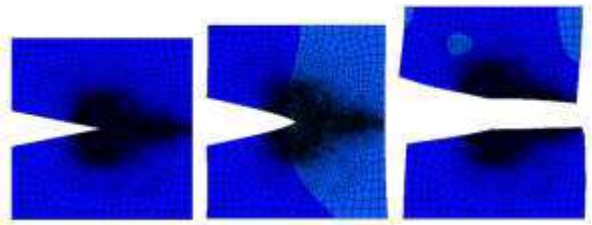

Fig. 18 FEA simulation of the crack propagation in an aged elastomer

References

Arruda EM, Boyce MC (1993) A three-dimensional constitutive model for the large stretch behavior of rubber elastic materials. Journal of the Mechanics and Physics of Solids 41:389–412. http://dx.doi.org/10.1016/0022-5096(93)90013-6

Ayoub G, Naït-Abdelaziz M, Zaïri F, et al (2011a) A continuum damage model for the high-cycle fatigue life prediction of styrene-butadiene rubber under multiaxial loading. International Journal of Solids and Structures 48:. https://doi.org/10.1016/j.ijsolstr.2011.04.003

Ayoub G, Rodriguez AK, Mansoor B, Colin X (2020) Modeling the visco-hyperelastic–viscoplastic behavior of photodegraded semi-crystalline low-density polyethylene films. International Journal of Solids and Structures 204–205:187–198. https://doi.org/10.1016/j.ijsolstr.2020.08.025

Ayoub G, Zaïri F, Naït-Abdelaziz M, Gloaguen JM (2011b) Modeling the low-cycle fatigue behavior of visco-hyperelastic elastomeric materials using a new network alteration theory: Application to styrene-butadiene rubber. Journal of the Mechanics and Physics of Solids 59:473–495. https://doi.org/10.1016/j.jmps.2010.09.016

Bahrololoumi A, Morovati V, Poshtan EA, Dargazany R (2020) A multi-physics constitutive model to predict hydrolytic aging in quasi-static behaviour of thin cross-linked polymers. International Journal of Plasticity 130:102676. https://doi.org/10.1016/j.ijplas.2020.102676

Balakhovsky K, Volokh KY (2012) Inflation and rupture of rubber membrane. Int J Fract 177:179–190. https://doi.org/10.1007/s10704-012-9764-5

Belbachir S, Zaïri F, Ayoub G, et al (2010) Modelling of photodegradation effect on elastic-viscoplastic behaviour of amorphous polylactic acid films. Journal of the Mechanics and Physics of Solids 58:. https://doi.org/10.1016/j.jmps.2009.10.003

Bolland JL (1949) Kinetics of olefin oxidation. Quarterly Reviews, Chemical Society 3:1. https://doi.org/10.1039/qr9490300001

Bouaziz R, Truffault L, Borisov R, et al (2020) Elastic Properties of Polychloroprene Rubbers in Tension and Compression during Ageing. Polymers 12:2354. https://doi.org/10.3390/polym12102354

Celina M, Gillen KT, Assink RA (2005) Accelerated aging and lifetime prediction: Review of non-Arrhenius behaviour due to two competing processes. Polymer Degradation and Stability 90:395–404. https://doi.org/10.1016/j.polymdegradstab.2005.05.004

Colclough T, Cunneen JI, Higgins GMC (1968) Oxidative aging of natural rubber vulcanizates. Part III. Crosslink scission in monosulfidic networks. Journal of Applied Polymer Science 12:295–307. https://doi.org/10.1002/app.1968.070120205

Colin X, Essatbi F, Delozanne J, Moreau G (2021) A new analytical model for predicting the thermal oxidation kinetics of composite organic m atrices. Application to diamine cross-linked epoxy. Polymer Degradation and Stability 186:109513

Colin X, Hassine MB, Nait-Abelaziz M (2019) Chemo-mechanical model for predicting the lifetime of epdm rubbers. Rubber Chemistry and Technology 92:722–748. https://doi.org/10.5254/rct.19.81469

Dal H, Kaliske M (2009) A micro-continuum-mechanical material model for failure of rubber-like materials: Application to ageing-induced fracturing. Journal of the Mechanics and Physics of Solids 57:1340–1356. https://doi.org/10.1016/j.jmps.2009.04.007

Dunn JR, Scanlan J (1961) Changes in the stress-strain properties of natural rubber vulcanizates during ageing. Transactions of the Faraday Society 57:160. https://doi.org/10.1039/tf9615700160

Fayolle B, Richaud E, Colin X, Verdu J (2008) Review: degradation-induced embrittlement in semi-crystalline polymers having their amorphous phase in rubbery state. J Mater Sci 43:6999–7012. https://doi.org/10.1007/s10853-008-3005-3

Flory PJ, Rehner Jr. J (1943) Statistical mechanics of cross-linked polymer networks I. Rubberlike elasticity. The Journal of Chemical Physics 11:512–520. https://doi.org/10.1063/1.1723791

Gent AN (1996) A New Constitutive Relation for Rubber. Rubber Chemistry and Technology 69:59–61. https://doi.org/10.5254/1.3538357

Horgan CO, Murphy JG (2009) On the volumetric part of strain-energy functions used in the constitutive modeling of slightly compressible solid rubbers. International Journal of Solids and Structures 46:3078–3085. https://doi.org/10.1016/j.ijsolstr.2009.04.007

Howse S, Porter C, Mengistu T, et al (2019) Experimental determination of the quantity and distribution of chemical crosslinks in unaged and aged natural rubber. II: A sulfur donor system. Rubber Chemistry and Technology 92:513–530

James HM, Guth E (1943) Theory of the elastic properties of rubber. The Journal of Chemical Physics 11:455–481. https://doi.org/10.1063/1.1723785

Jernigan RL, Flory PJ (1969) Distribution functions for chain molecules. The Journal of Chemical Physics 50:4185–4200. https://doi.org/10.1063/1.1670884

Kadri R, Nait Abdelaziz M, Fayolle B, et al (2022) A unified mechanical based approach to fracture properties estimates of rubbers subjected to aging. International Journal of Solids and Structures 234:111305

Kaliske M, Heinrich G (1999) An Extended Tube-Model for Rubber Elasticity: Statistical-Mechanical Theory and Finite Element Implementation. Rubber Chemistry and Technology 72:602–632. https://doi.org/10.5254/1.3538822

Kashi S, Varley R, De Souza M, et al (2018) Mechanical, Thermal, and Morphological Behavior of Silicone Rubber during Accelerated Aging. Polymer-Plastics Technology and Engineering 57:1687–1696. https://doi.org/10.1080/03602559.2017.1419487

Kuhn W, Grun F (1942) Relationships between elastic constants and stretching double refraction of highly elastic substances. Kolloid Z 101:

Lake GJ (2003) Fracture mechanics and its application to failure in rubber articles. Rubber chemistry and technology 76:567–591

Lavoie SR, Long R, Tang T (2019) Modeling the mechanics of polymer chains with deformable and active bonds. The Journal of Physical Chemistry B 124:253–265

Le Gac PY, Choqueuse D, Melot D (2013) Description and modeling of polyurethane hydrolysis used as thermal insulation in oil offshore conditions. Polymer Testing 32:1588–1593. https://doi.org/10.1016/j.polymertesting.2013.10.009

Li B, Bouklas N (2020) A variational phase-field model for brittle fracture in polydisperse elastomer networks. International Journal of Solids and Structures 182:193–204

Mao Y, Talamini B, Anand L (2017) Rupture of polymers by chain scission. Extreme Mechanics Letters 13:17–24

Marckmann G, Verron E, Gornet L, et al (2002) A theory of network alteration for the Mullins effect. Journal of the Mechanics and Physics of Solids 50:2011–2028. https://doi.org/10.1016/S0022-5096(01)00136-3

Mark JE;, Tang MY; (1984) Dependence of the elastomeric properties of bimodal networks on the lengths and amounts of the short chains. Journal of Polymer Science: Polymer Physics 22:1849–1855

Meyer KH, Ferri C (1935) Sur l'élasticité du caoutchouc. Helvetica Chimica Acta 18:570–589. https://doi.org/10.1002/hlca.19350180176

Miehe C, Göktepe S, Lulei F (2004) A micro-macro approach to rubber-like materials - Part I: The non-affine micro-sphere model of rubber elasticity. Journal of the Mechanics and Physics of Solids 52:2617–2660. https://doi.org/10.1016/j.jmps.2004.03.011

Mooney M (1940) A theory of large elastic deformation. Journal of Applied Physics 11:582–592. https://doi.org/10.1063/1.1712836

Nait Abdelaziz M, Ayoub G, Colin X, et al (2019) New developments in fracture of rubbers: Predictive tools and influence of thermal aging. International Journal of Solids and Structures 165:127–136. https://doi.org/10.1016/j.ijsolstr.2019.02.001

Planes E, Chazeau L, Vigier G, et al (2010a) Influence of fillers on mechanical properties of ATH filled EPDM during ageing by gamma irradiation. Polymer Degradation and Stability 95:1029–1038. https://doi.org/10.1016/j.polymdegradstab.2010.03.008

Planes E, Chazeau L, Vigier G, et al (2010b) Influence of fillers on mechanical properties of ATH filled EPDM during ageing by gamma irradiation. Polymer Degradation and Stability 95:1029–1038. https://doi.org/10.1016/j.polymdegradstab.2010.03.008

Planes E, Chazeau L, Vigier G, Fournier J (2009) Evolution of EPDM networks aged by gamma irradiation – Consequences on the mechanical properties. Polymer 50:4028–4038. https://doi.org/10.1016/j.polymer.2009.06.036

Pourmand P, Hedenqvist MS, Furo I, Gedde UW (2017) Deterioration of highly filled EPDM rubber by thermal ageing in air: Kinetics and non-destructive monitoring. Polymer Testing 64:267–276

Rincon-Rubio LM, Fayolle B, Audouin L, Verdu J (2001) A general solution of the closed-loop kinetic scheme for the thermal oxidation of polypropylene. Polymer Degradation and Stability 74:177–188. https://doi.org/10.1016/S0141-3910(01)00154-9

Rodriguez AK, Mansoor B, Ayoub G, et al (2020) Effect of UV-aging on the mechanical and fracture behavior of low density polyethylene. Polymer Degradation and Stability 180:109185

Tehrani M, Sarvestani A (2017) Effect of chain length distribution on mechanical behavior of polymeric networks. European Polymer Journal 87:136–146

Trapper P, Volokh KY (2010) Modeling dynamic failure in rubber. Int J Fract 162:245–253. https://doi.org/10.1007/s10704-010-9448-y

Treloar LRG (1946) The elasticity of a network of long-chain molecules.—III. Trans Faraday Soc 42:83–94. https://doi.org/10.1039/TF9464200083

Vernerey FJ, Brighenti R, Long R, Shen T (2018) Statistical Damage Mechanics of Polymer Networks. Macromolecules 51:6609–6622. https://doi.org/10.1021/acs.macromol.8b01052

Volokh KY (2007) Hyperelasticity with softening for modeling materials failure. Journal of the Mechanics and Physics of Solids 55:2237–2264. https://doi.org/10.1016/j.jmps.2007.02.012

Wang MC, Guth E (1952) Statistical Theory of Networks of Non-Gaussian Flexible Chains. The Journal of Chemical Physics 20:1144–1157. https://doi.org/10.1063/1.1700682

Yeoh OH (1990) Characterization of Elastic Properties of Carbon-Black-Filled Rubber Vulcanizates. Rubber Chemistry and Technology 63:792–805. https://doi.org/10.5254/1.3538289

Appendix A

The kirchhoff stress is obtained by adding the hydrostatic and the deviatoric contributions:

$$\boldsymbol{\tau} = p\mathbf{g}^{-1} + \mathbf{P} : \bar{\boldsymbol{\tau}}$$

Where $\mathbf{P}$ is the fourth-order identity tensor:

$$\mathbf{P}^{ab}_{cd} = \frac{\left[\delta^a_c \delta^b_d + \delta^a_d \delta^b_c\right]}{2} - \frac{1}{3}\delta^{ab}\delta_{cd}$$

With δ being the Kronecker-delta symbol.

The hydrostatic stress p is obtained through the derivative of the volumetric part U of the free energy :

$$p = J\frac{\partial U(J)}{\partial J}$$

U is an incompressibility constraint that can take different forms (Horgan and Murphy 2009) and is considered as a penalty function to approach the incompressible response.

The deviatoric stress $\bar{\boldsymbol{\tau}}$ is derived from the isochoric part of the free energy function $\overline{\Psi}$ by using the intermediate derivative (i.e $2\partial\lambda / \partial\mathbf{g} = \lambda^{1-q}\mathbf{h}$ with $\mathbf{h} = \langle \bar{\lambda}^{q-2}\mathbf{t}\otimes\mathbf{t}\rangle$) (Miehe et al. 2004):

$$\bar{\boldsymbol{\tau}} = 2\frac{\partial \overline{\Psi}(\mathbf{g};\bar{\mathbf{F}})}{\partial \mathbf{g}} = \overline{\Psi}'\ \lambda^{1-q}\mathbf{h}$$

Where q is the non-affinity parameter between micro and macro stretch.

$\overline{\Psi}' = nf$ is the single elastic potential derivation and f is the micro force defined as $f = \partial\psi / \partial\lambda$.

Since we are assuming a series scheme, the stress in each spring is assumed to be equal to the total stress, and hence λ_η and λ_e are computed by using the following relation:

$$f_\eta \lambda_\eta - f_e \lambda_e = 0$$

$f_\eta = \partial\psi_\eta / \partial\lambda_\eta$ and $f_e = \partial\psi_e / \partial\lambda_e$ being the entropic and bond micro forces, respectively.

The problem can be solved using any iterative scheme. In this work, a Newton-type procedure is used to solve the residual quantity $r = f_\eta \lambda_\eta - f_e \lambda_e \approx 0$.

Once the different micro-stretch contributions are determined, the isochoric kirchhoff stress $\bar{\boldsymbol{\tau}}$ can be computed:

$$\bar{\boldsymbol{\tau}} = 2n \frac{\partial\lambda}{\partial \mathbf{g}} \left[\frac{\partial\psi_\eta}{\partial\lambda_\eta} \frac{\partial\lambda_\eta}{\partial\lambda} + \frac{\partial\psi_e}{\partial\lambda_e} \frac{\partial\lambda_e}{\partial\lambda} \right] = n \left(f_\eta \frac{\partial\lambda_\eta}{\partial\lambda} + f_e \frac{\partial\lambda_e}{\partial\lambda} \right) \lambda^{1-q} \mathbf{h}$$

The partial derivative $\partial\lambda_\eta / \partial\lambda$ and $\partial\lambda_e / \partial\lambda$ are determined using the following equalities:

$$\frac{dr}{d\lambda} = \frac{\partial r}{\partial\lambda} + \frac{\partial r}{\partial\lambda_\eta} \frac{\partial\lambda_\eta}{\partial\lambda} = 0$$

Finally, the following simplified forms are obtained:

$$\frac{\partial\lambda_\eta}{\partial\lambda} = \frac{\bar{\square}_e}{\lambda_\eta \bar{\square}_\eta + \lambda_e \bar{\square}_e} \qquad \text{and} \qquad \frac{\partial\lambda_e}{\partial\lambda} = \frac{\bar{\square}_\eta}{\lambda_\eta \bar{\square}_\eta + \lambda_e \bar{\square}_\eta}$$

Where

$$\bar{\square}_\eta = f_\eta + \lambda_\eta \frac{\partial f_\eta}{\partial\lambda_\eta} \qquad \text{and} \qquad \bar{\square}_e = f_e + \lambda_e \frac{\partial f_e}{\partial\lambda_e}$$

Appendix B

Table. 4 Parameter of the EAC density $n(t)$ evolution equation.

Materials	b_1	b_2	b_3	b_4
EPDM01	0.9	0.009	0.258	0
EPDM02	0.789	$-2.28\ 10^{-3}$	0.398	0.1086
PU	1.8310^{21}	$-4.5\ 10^{-2}$	0	0
SR	$5.12\ 10^{19}$	$-5.896\ 10^{-2}$	0	0